

Table S1. Forcings for assessing the long-term Antarctic sea-level commitment in terms of projected atmospheric temperature change at different points in time. Antarctic-averaged atmospheric temperature change with respect to mean over time period 1995-2014 at different points in time under emission pathways SSP1-2.6 and SSP5-8.5 projected by four CMIP6 GCMs used to force the ice-sheet models. For a given point in time, upper rows represent SSP1-2.6 and lower rows correspond to SSP5-8.5. The corresponding Antarctic sea-level commitment is determined with all ice-sheet model configurations given in Table S2.

		MRI-ESM2-0	CESM2-WACCM	IPSL-CM6A-LR	UKESM1-0-LL
2050	SSP1-2.6	0.90	1.26	1.54	1.34
	SSP5-8.5	1.38	1.90	1.85	1.86
2100	SSP1-2.6	1.38	2.43	1.56	1.26
	SSP5-8.5	5.02	6.35	5.30	6.20
2150	SSP1-2.6	1.77	2.50	1.10	1.35
	SSP5-8.5	8.50	10.47	8.99	9.66
2200	SSP1-2.6	1.89	2.86	1.16	1.39
	SSP5-8.5	10.70	13.36	11.67	11.80
2250	SSP1-2.6	2.26	2.81	1.44	1.18
	SSP5-8.5	11.57	15.14	13.39	13.05
2300	SSP1-2.6	2.36	3.58	0.98	1.22
	SSP5-8.5	12.14	16.4	14.08	13.52

Table S2. Ice-sheet model configurations. Ice-sheet model configurations used for assessing the long-term Antarctic sea-level commitment. While initial ice-sheet conditions with Kori-ULB are obtained in an inverse simulation for each of the atmospheric climatologies, these are derived from a spin-up ensemble for each atmospheric climatology in PISM. The combinations of PISM parameters for the initial ice-sheet states selected from these ensembles are given as well.

	Atmospheric climatology	Sliding exponent	SIA enhancement factor	Tillwater decay rate	Till effective overburden fraction
Kori-ULB	MARv3.11	-	-	-	-
	RACMO2.3p2	-	-	-	-
PISM	MARv3.11	0.75	2.0	7 mm yr ⁻¹	0.015
	RACMO2.3p2	0.5	1.5	7 mm yr ⁻¹	0.015

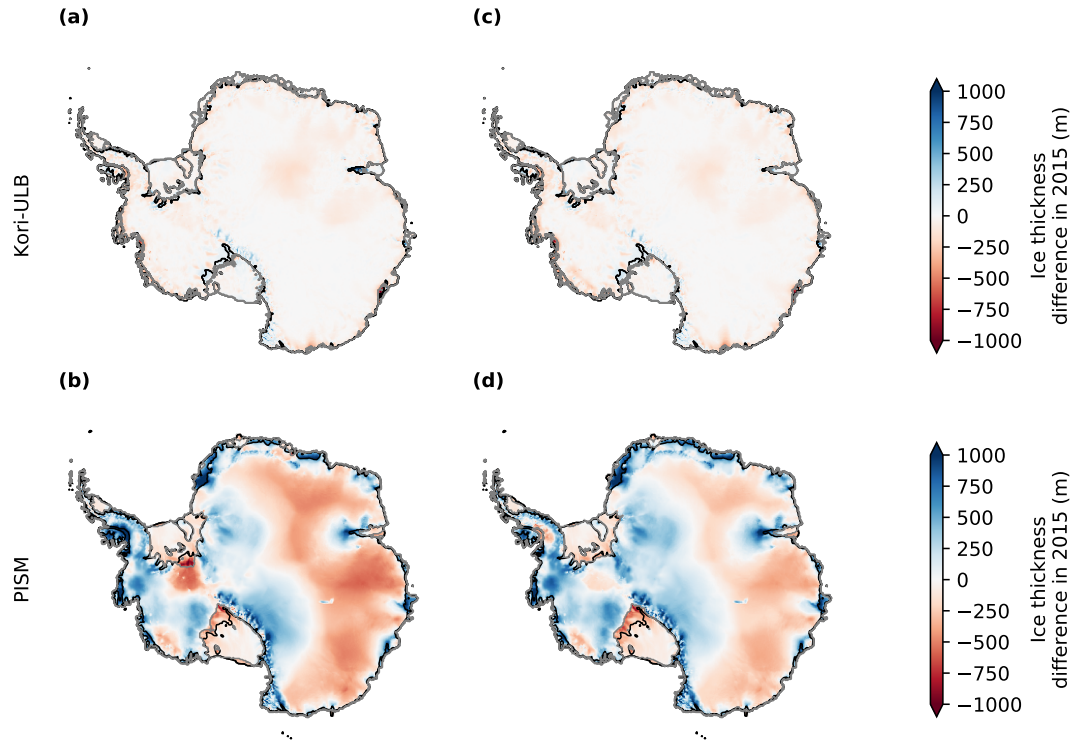


Figure S1. Comparison between modelled and observed ice-sheet geometry. Modelled present-day ice thickness in the ice-sheet models Kori-ULB (upper row) and PISM (lower row), using atmospheric climatologies based on MAR (left column) and RACMO (right column) relative to observed ice thickness in present-day (Bedmachine for Kori-ULB and Bedmap2 for PISM). Modelled and observed grounding line and calving front position are shown in grey and black, respectively. Note the different scales of the colourbar for Kori-ULB and PISM.

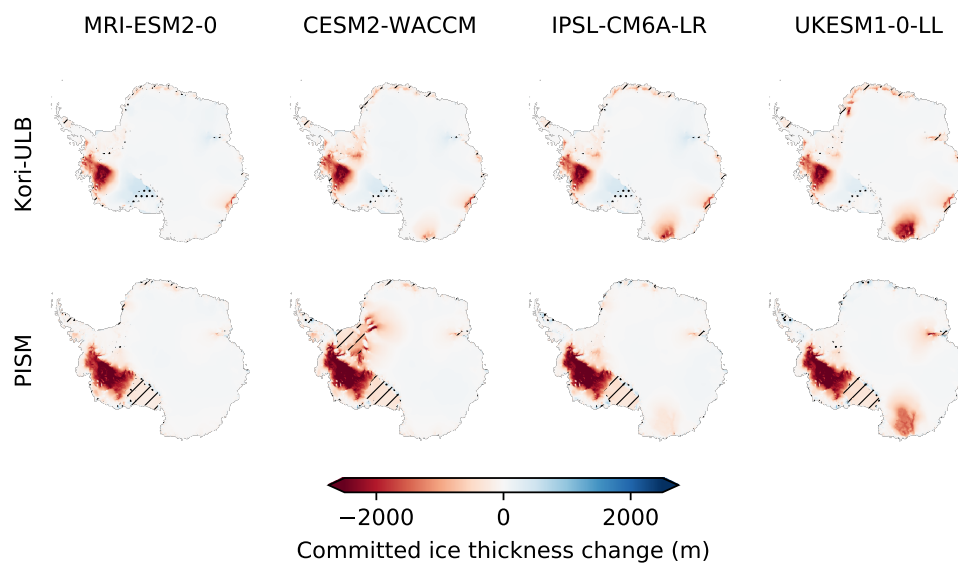


Figure S2. Committed ice-sheet responses to changing climate conditions under the lower-emission pathway SSP1-2.6. Shown is the mean ice-thickness change in the year 7000 depending on the applied CMIP6 GCMs, as determined by the ice-sheet models Kori-ULB (upper row) and PISM (lower row). For each ice-sheet model, the ice-thickness change is averaged across all branchoff points in time and the respective ice-sheet model configurations (Table S2). A potential loss of ice shelves is indicated by hatching. Dots mark areas of potential ice-sheet advance.

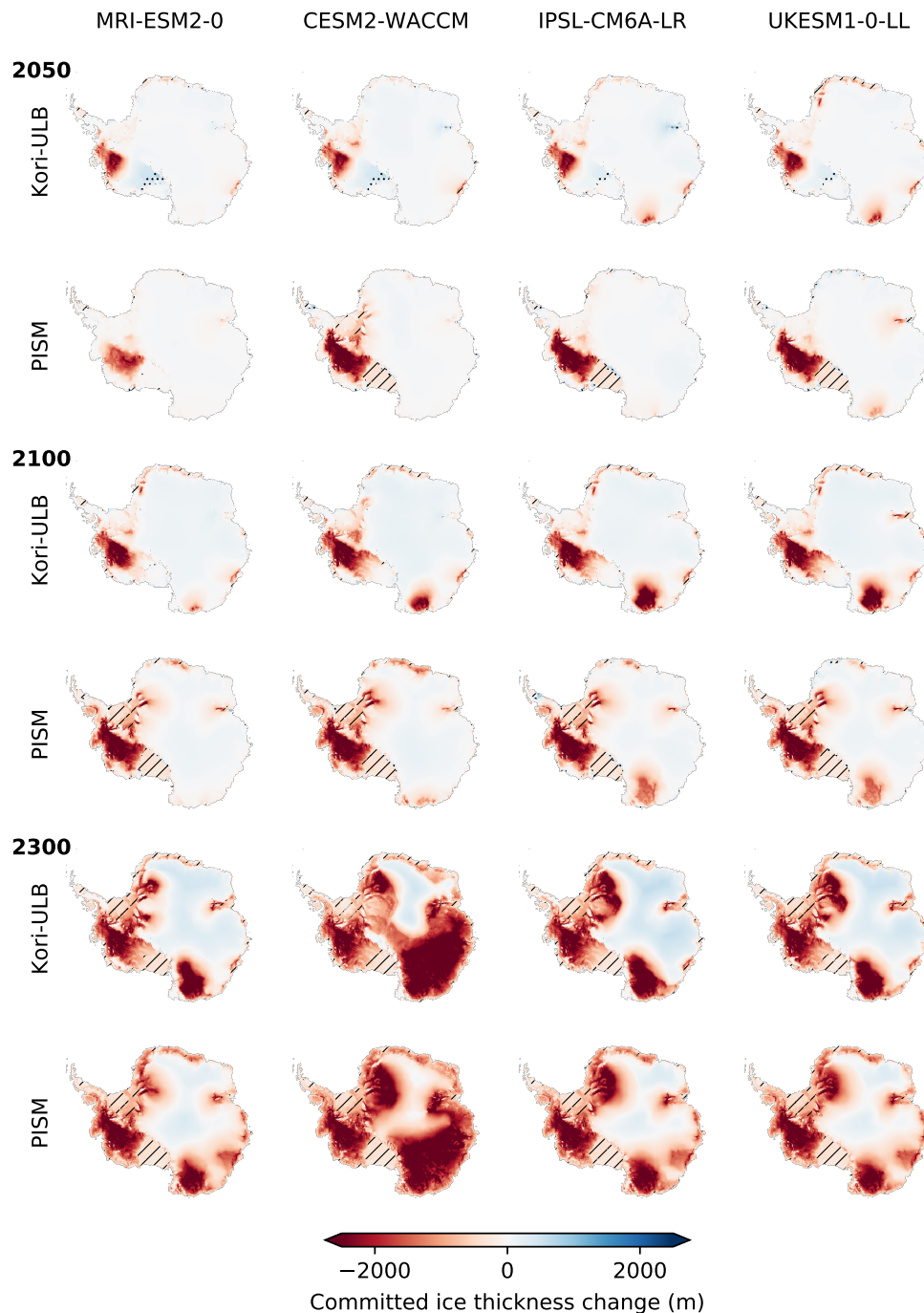


Figure S3. Committed ice-sheet responses to changing climate conditions under the higher-emission pathway SSP5-8.5. Shown is the mean-ice thickness change in the year 7000 when stabilizing climatic boundary conditions in the years 2050, 2100 and 2300 (from top to bottom) depending on the applied CMIP6 GCMs, as determined by the ice-sheet models Kori-ULB and PISM. For each ice-sheet model, the ice-thickness change is averaged across the respective ice-sheet model configurations (Table S2). A potential loss of ice shelves is indicated by hatching. Dots mark areas of potential ice-sheet advance.

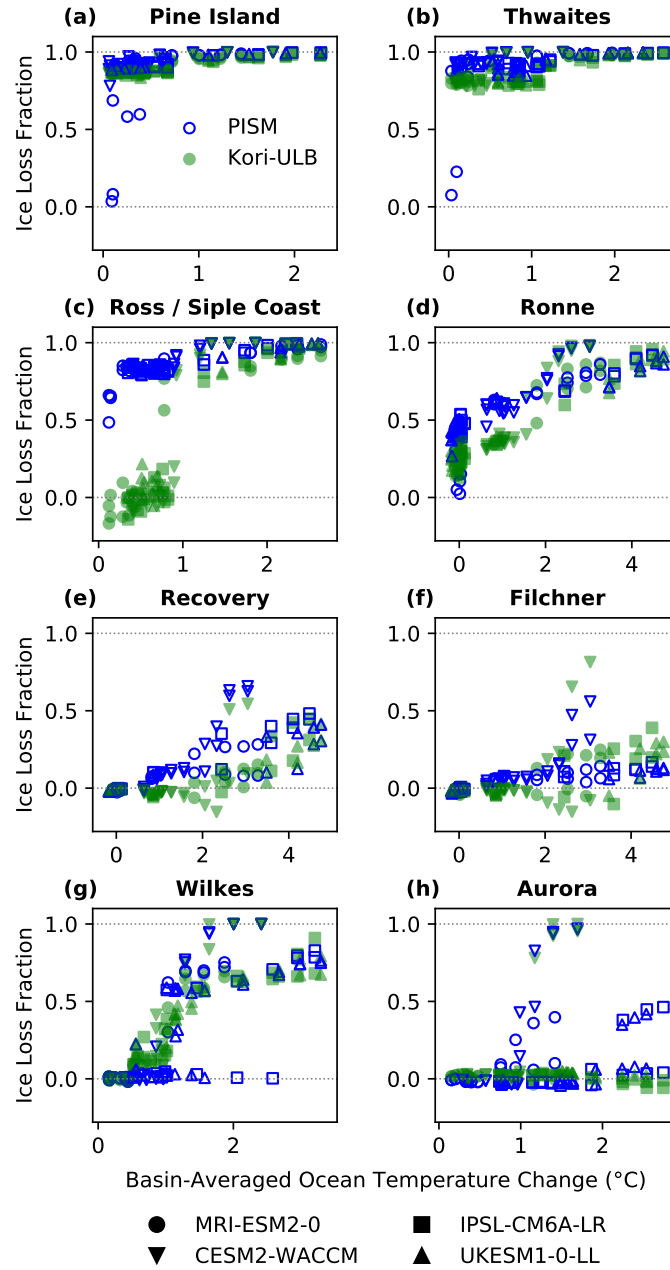


Figure S4. Ice loss from Antarctic drainage basins depending on ocean temperature change. Long-term ice loss from different Antarctic drainage basins (as fraction of respective sea-level rise potential) for the year 7000 in response to basin-averaged ocean temperature change (compared to 1995–2014) projected by four CMIP6 GCMs (given by marker shape). Filled green and open blue markers correspond to the long-term ice loss determined by the ice-sheet models Kori-ULB and PISM, respectively.